Available online at www.sciencedirect.com
ScienceDirect
Journal of Organometallic Chemistry 691 (2006) 5576–5584
Journal of Organometallic Chemistry
www.elsevier.com/locate/jorganchem

Dynamic behaviour of 1,*n*′-disubstituted ferrocenes

Katja Heinze *, Manuela Beckmann

Department of Inorganic Chemistry, University of Heidelberg, Im Neuenheimer Feld 270, 69120 Heidelberg, Germany

Received 8 August 2006; accepted 29 August 2006
Available online 15 September 2006

Abstract

1,*n*′-Disubstituted ferrocenes with ketone/phthalimido (**2**) and ketone/amine substituents (**3**) were synthesised and characterised by IR, ^{1}H NMR, ^{13}C NMR, VT ^{1}H NMR, UV/Vis spectroscopy, mass spectrometry and cyclic voltammetry. The molecular structure of **2** was confirmed by X-ray crystal structure determination. The dynamic behaviour was experimentally studied in solution and theoretically by DFT calculations. The thermal stability of the ketone/amine derivative **3** was investigated using thermal analyses.

Keywords: Conformational analysis; Electronic structure; Ferrocene; Modelling; Thermal analysis

1. Introduction

Unsymmetrical 1,*n*′-disubstituted ferrocenes [1,2] are useful building blocks for directional oligomers with ferrocene in the main chain or as starting materials for (chiral) ferrocene-containing chelating ligands potentially applicable in (asymmetric) catalysis [3–15].

Recently we reported the synthesis of *N*-Fmoc protected 1,*n*′-disubstituted ferrocene amino acid (*N*-Fmoc-Fca) as building block for ferrocene containing peptides [16]. Such artificial peptides could find applications as sensors, molecular wires and optical materials in molecular recognition, molecular electronics and molecular optics [17–19].

Herein we present the synthesis, characterisation and a combined experimental and theoretical study of the dynamic behaviour and thermal stability of 1,*n*′-disubstituted ferrocenes with ketone/phthalimido and ketone/amine substituents.

2. Results and discussion

To selectively obtain 1,*n*′-disubstituted ferrocenes 2-ferrocenylisoindole-1,3-dione **1** [16] is reacted with 2,6-dichlorobenzoyl chloride in a Friedel–Crafts acylation to give 1-phthalimido-*n*′-(2,6-dichlorobenzoyl)-ferrocene **2** which is further transformed into the amine **3** by reaction with hydrazine (Scheme 1).

The successful Friedel Crafts acylation of **1** is confirmed by the IR spectrum of **2** in CH_2Cl_2 which displays characteristic IR absorption bands in the *ν*(CO) region for the symmetric and asymmetric CO stretching vibrations of the phthalimido substituent and an additional band at 1658 cm^{-1} for the ketone group at the second Cp ring. None of these signals is significantly shifted in the solid state ruling out any strong contacts between these groups and possible proton donors (see below).

The absence of signals for the phthalimido substituent and the presence of absorption bands of NH stretching vibrations in the IR spectra of **3** prove the desired transformation of the phthalimido substituent into the amine functionality. The signals for the symmetric and asymmetric NH stretching vibrations shift to lower energy by 45 and 47 cm^{-1} when going from the solution to the solid state (CH_2Cl_2: $\nu = 3434$, 3362 cm^{-1}; solid: $\nu = 3389$, 3315 cm^{-1}). For aminoferrocene $FcNH_2$ displaying weak NH···N hydrogen bonds in the crystal the corresponding signals shift by only 25 and 18 cm^{-1} (CH_2Cl_2: $\nu = 3425$, 3354 cm^{-1}; solid: $\nu = 3400$, 3336 cm^{-1}) [16]. Furthermore in solution the signal for the CO_{ketone} vibration for **3** is very

* Corresponding author. Fax.: +49 6221 545707.
E-mail address: katja.heinze@urz.uni-heidelberg.de (K. Heinze).

0022-328X/$ - see front matter © 2006 Elsevier B.V. All rights reserved.
doi:10.1016/j.jorganchem.2006.08.096

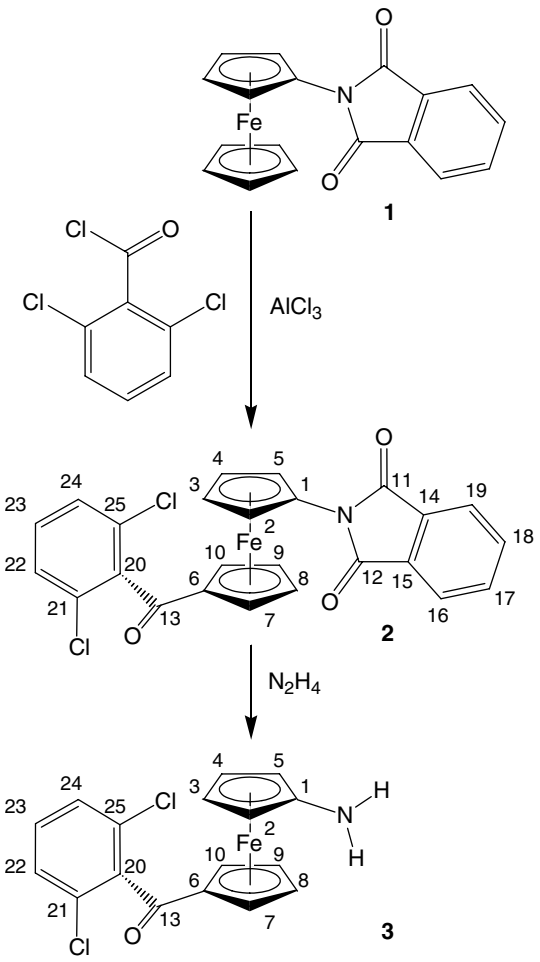

Scheme 1. Synthesis of **2** and **3** and atom numbering scheme.

similar to that observed for **2**. In the solid state, however, the CO_{ketone} absorption for **3** is bathochromically shifted by 21 cm^{-1} as compared to that of **2**. These observations together suggest a hydrogen-bonded structure of **3** with NH···O=C hydrogen bonds in the solid state (probably intermolecular in nature).

NMR spectroscopy additionally confirms the successful formation of **2** and **3**, respectively. All proton and carbon signals of **2** and **3** have been assigned by 2D NMR spectroscopy, literature comparison [16] and simulation of the coupling patterns (H^{22-24}, H^{16-19}). The amine protons of **3** resonate at $\delta = 2.74$ in CD_2Cl_2, almost independent of temperature and only slightly shifted to lower field as compared to those of aminoferrocene $FcNH_2$ ($\delta = 2.63$ [16]).

Ferrocene **2** with two sterically demanding substituents was studied by variable-temperature ^1H NMR spectroscopy in CD_2Cl_2 to probe its conformational flexibility (Fig. 1). At 243 K the signal of $H^{7/10}$ broadens until coalescence is reached at 203 K. Similarly, the signal for $H^{8,9}$ broadens at 223 K. Unfortunately, the slow-exchange limit could not be reached at 400 MHz operating frequency. However, the activation energy can be estimated to be around 35–40 kJ mol^{-1} [16]. Thus a dynamic process involving the rotation of the aromatic ketone around the

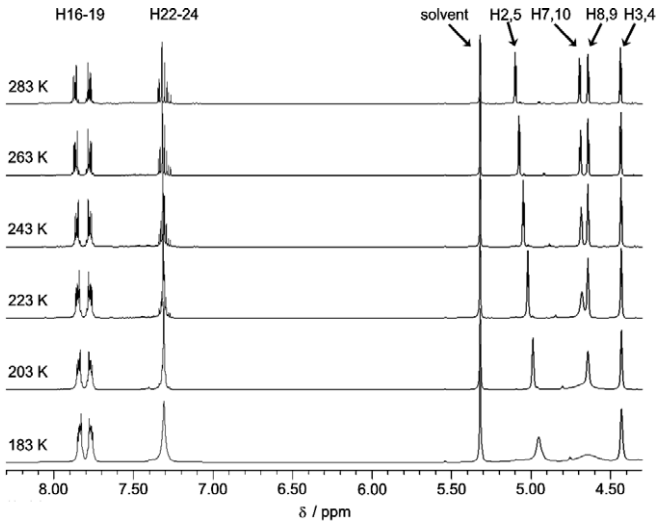

Fig. 1. VT ^1H NMR of **2** in CD_2Cl_2 at 400 MHz.

C^6–C^{13} vector which discriminates H^7/H^{10} and H^8/H^9 is proposed (see Scheme 1 for atom numbering). The potential barrier for the sterically less encumbered benzoyl ferrocene has been determined as 28 kJ mol^{-1} [20]. Unfortunately, amine **3** shows only general broadening of all signals due to beginning precipitation at lower temperatures preventing any barrier estimation.

To support the interpretations DFT calculations have been performed first for the equilibrium structures of **2** and then for possible transition states for the aryl ketone rotation in **2** (Table 1). The 1,3′ conformation of the disubstituted ferrocene minimises steric repulsion between the rather large substituents but still allows an eclipsed conformation of the Cp rings thus representing the most stable geometry of **2** (1,3′a and 1,3′b; see X-ray structure of **2** below). However, the 1,1′ and 1,2′ conformations are only slightly higher in energy resulting in an almost unhindered rotation of the Cp rings in solution. In the 1,2′ and 1,3′ conformers the phthalimido and the ketone group are almost co-planar to the Cp rings to which they are attached (torsion angles C2–C1–N1–C12 and O3–C13–C6–C7, Table 1) while the dichloro aryl ring is oriented rather perpendicular to the keto group due to steric congestion imposed by the chloro substituents (torsion angle O3–C13–C20–C21, Table 1).

Rotation of the aryl ketone moiety was modelled both in the 1,1′ and 1,3′ conformations (Figs. 2 and 3). In the 1,1′ rotamers steric interactions between the substituents in the nearly C_s-symmetric transition state 1,1′TS raise the activation barrier (>55 kJ mol^{-1}, Fig. 2) while aryl ketone rotation in the 1,3′ conformers requires only 34–41 kJ mol^{-1} (1,3′TS1 and 1,3′TS2; Fig. 3) which fits to the barrier estimation from the VT NMR data. The reason for the still quite high barrier – as compared e.g. to the low barrier for acetyl amido substituted ferrocenes (<20 kJ mol^{-1} [18]) – is the beginning double bond localisation between C^6/C^{13} (C^6–C^{13} 1.470 Å, C^{13}–C^{20} 1.525 Å) and in the Cp ring C^{6-10} (C^6–C^7, C^6–C^{10} 1.451 Å; C^7–C^8, C^9–C^{10}

Table 1
Selected properties of DFT optimised geometric structures of **2** and **3**

Rotamer	E_{rel}/kJ mol^{-1}	ν_{imag}/cm^{-1}	Torsion angle/° O3–C13–C6–C7	Torsion angle/° O3–C13–C20–C21	Torsion angle/° C2–C1–N1–C12	C^6–C^{13}/Å
2						
1,1′a	6.4	–	158.5	105.9	27.1	1.470
1,1′b	6.1	–	21.5	−105.7	−25.2	1.470
1,1′TS	63.5	75.8i cm^{-1}	88.8	179.9	8.3	1.497
1,2′a	10.8	7.0i cm^{-1}[a]	173.6	108.8	−7.6	1.471
1,2′b	2.9	–	10.5	71.5	−22.8	1.470
1,3′a	<1.0	–	170.9	104.3	5.2	1.470
1,3′b	0.0	–	10.9	71.2	2.5	1.470
1,3′TS1	34.3	28.8i cm^{-1}	91.5	89.4	1.9	1.495
1,3′TS2	41.8	19.9i cm^{-1}	−86.0	88.5	9.7	1.498
3					Torsion angle/° C2–C1–N1–H	
1,1′b	0	–	19.4	70.6	15.9	1.463
1,3′b	5.9	–	8.0	70.4	3.0	1.466

[a] This frequency corresponds to the Cp ring rotation.

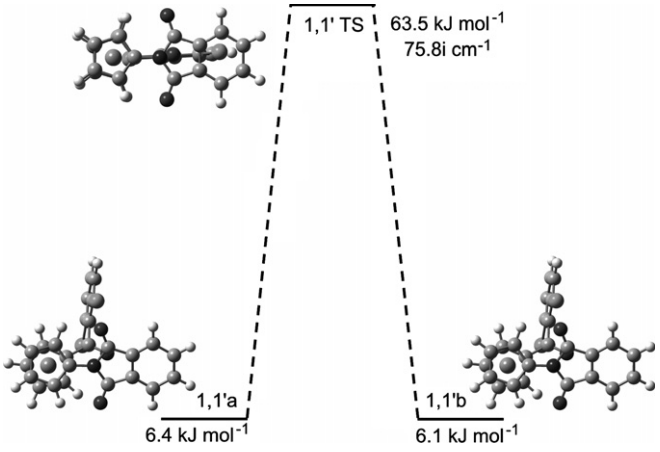

Fig. 2. Energy profile for the aryl ketone rotation in the 1,1′ conformer of **2** (view approximately perpendicular to the Cp planes).

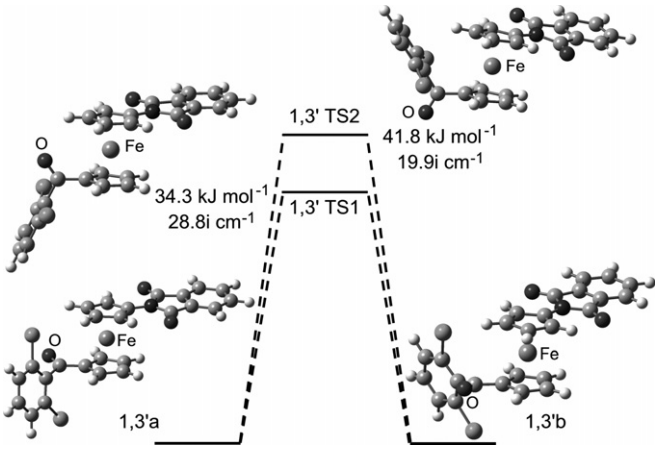

Fig. 3. Energy profile for the aryl ketone rotation in the 1,3′ conformer of **2**.

1.434 Å; C^8–C^9 1.447 Å) which has been noted previously for structurally characterised acyl substituted ferrocenes [21]. Thus rotation of the aryl keto group is hindered even in the 1,3′ conformer due to the partial double bond character of the C^6–C^{13} bond which is reduced in the transition states 1,3′TS1 (C^6–C^{13} 1.495 Å) and 1,3′TS2 (C^6–C^{13} 1.498 Å) (Fig. 3).

In contrast to **2** for the amine **3** the 1,1′ conformation of the ferrocene is slightly more stable than the 1,3′ conformation (Fig. 4, Table 1) in spite of the fact that the aryl ketone substituent is no more coplanar to the Cp ring to which it is attached (torsion angle O3–C13–C6–C7 19.4°). However, double bond localisation seems to be only marginally influenced by this distortion (C^6–C^{13} 1.463 Å; C^{13}–C^{20} 1.527 Å; C^6–C^7 1.453 Å; C^6–C^{10} 1.454 Å; C^7–C^8 1.435 Å; C^9–C^{10} 1.432 Å; C^8–C^9 1.446 Å). In fact, in the 1,1′ rotamer additional contacts are observed between the amine protons and the aryl ketone substituent (Fig. 4) namely $O^3\cdots H_{amine}$ and $Cl^2\cdots H_{amine}$ contacts which might stabilise the 1,1′ conformer with respect to the 1,3′ conformer. This stabilisation, however, is only very weak and in solution a dynamic mixture of conformers is expected consistent with IR and NMR data.

The electronic and redox properties of **2** and **3** have been analysed by UV/Vis spectroscopy, cyclic voltammetry and

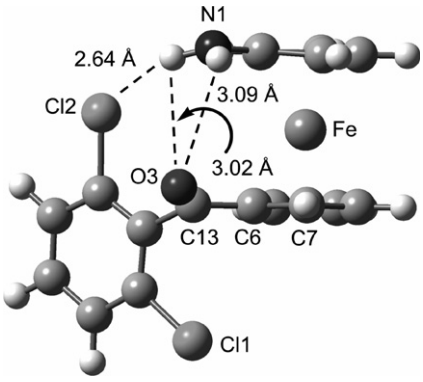

Fig. 4. DFT optimised structure of **3** (1,1′ rotamer; view approximately parallel to the Cp planes with short contacts indicated by dashed lines).

DFT calculations. Both compounds **2** and **3** display a bathochromically shifted ferrocene absorption at $\lambda_{max} =$ 471 nm (**2**) and $\lambda_{max} = 493$ nm (**3**) as compared to that of ferrocene ($\lambda_{max} = 440$ nm). This effect arises from mixing of substituent orbitals into the frontier orbitals of the ferrocene moiety, which is especially pronounced for mixing aryl ketone character into the virtual orbitals (Fig. 5). For **2** an additional molecular orbital (LUMO) – basically localised on the phthalimido substituent and barely influencing the ferrocene transition – is inserted in the frontier orbital region. The electron-donating character of the amine substituent in **3**, however, raises the energies of the occupied d_π(Fe) orbitals resulting in a smaller energy gap of this push–pull substituted ferrocene (**2**: $\Delta E_{HOMO/LUMO+1} =$ 4.0 eV; **3**: $\Delta E_{HOMO/LUMO} = 3.7$ eV) consistent with the experimental results. The bathochromic shift is accompanied by a hyperchromic effect caused by the symmetry-lowering interaction of the cyclopentadienyl π orbitals with the substituents. This mixing induces some charge-transfer character and raises the extinction coefficients of the transitions from 100 $M^{-1}\,cm^{-1}$ (ferrocene) to 650 $M^{-1}\,cm^{-1}$ (**2**) and 905 $M^{-1}\,cm^{-1}$ (**3**).

Compounds **2** and **3** are reversibly oxidised at 0.77 V (**2**) and 0.38 V (**3**) and irreversibly reduced at $E_p = -1.3$ V and −1.4 V (Fig. 6). A follow-up reaction (probably pinacol formation [22–27]) is coupled to the reduction processes giving rise to new oxidation waves at 0.52 V and 0.16 V for **2** and **3**, respectively. The electron accepting character of both substituents in **2** results in its quite positive oxidation potential. This effect is compensated for by the electron donating effect of the amine group in **3** shifting the potential towards lower values by 0.39 V. A similar shift (0.32 V) has been observed in the pair **1**/$FcNH_2$ [16]. Such

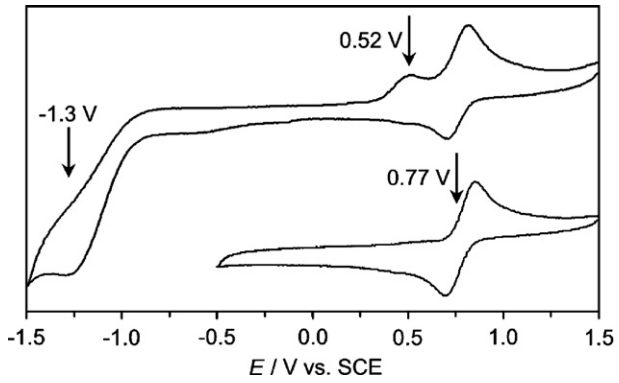

Fig. 6. Cyclic voltammograms of **2**.

additive effects of substituents on the redox potential were previously observed and parameterised for numerous ferrocene derivatives [28].

The molecular structure of **2** has been confirmed by a single crystal structure analysis (Fig. 7, Table 2). Compound **2** crystallises in the orthorhombic space group $Pna2_1$ with four molecules in the unit cell. The crystal examined was a racemic twin with Flack $x = 0.36(4)$. As expected from the IR data no intermolecular contacts are observed in the crystalline state.

The experimentally observed molecular structure of **2** confirms the DFT calculated minimum geometry with the 1,3′ conformation being the most stable one. Even the conformation of the aryl ketone moiety [O^3–C^{13}–C^6–C^7 175.03(0.62)°; O3–C13–C20–C21 111.36(0.75)°; Tables 1 and 2] and the beginning double bond localisation in the Cp ring C6–C10 [C^6–C^{13} 1.461(9) Å; C^{13}–C^{20} 1.504(10) Å; C^6–C^7 1.438(9) Å; C^6–C^{10} 1.443(10) Å; C^7–C^8 1.416(10)

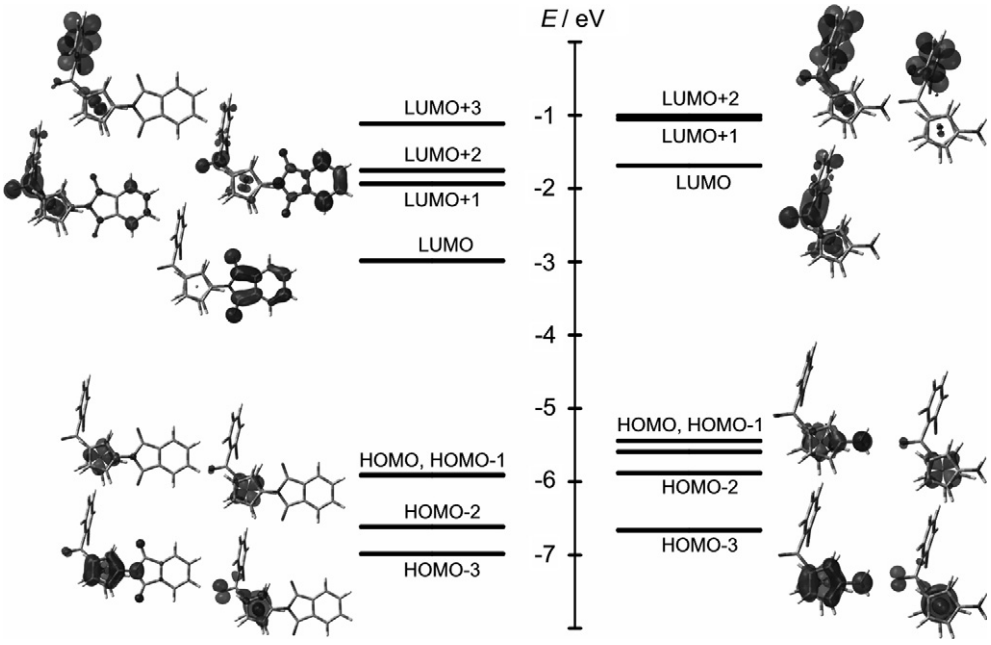

Fig. 5. Molecular orbitals of **2** (left) and **3** (right) (B3LYP, LanL2DZ; 1,3′a rotamers; displayed at an isosurface value of 0.04; view approximately perpendicular to the Cp planes).

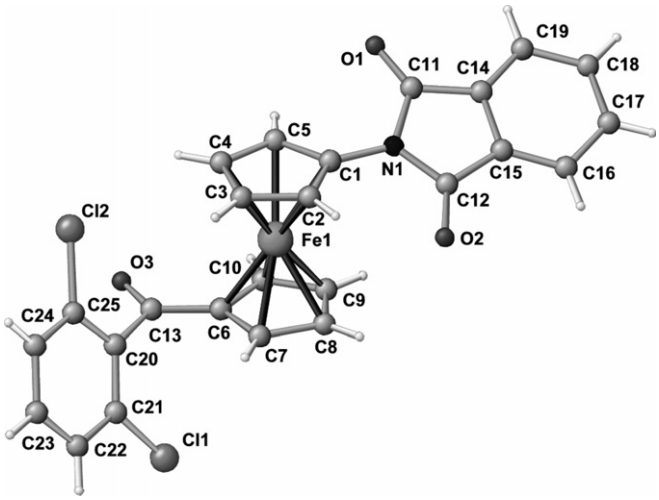

Fig. 7. Molecular structure of **2** in the crystal.

Table 2
Selected bond lengths (Å) and angles (°) of **2**

Bond lengths/Å		Bond angles/°	
Fe1–C1	2.070(7)	C1–N1–C11	123.1(6)
Fe1–C2	2.060(5)	C1–N1–C12	126.5(6)
Fe1–C3	2.028(6)	C11–N1–C12	110.5(6)
Fe1–C4	2.048(7)	C6–C13–O3	122.2(6)
Fe1–C5	2.066(7)	C6–C13–C20	118.9(6)
Fe1–C6	2.049(6)	O3–C13–C20	119.0(6)
Fe1–C7	2.035(7)		
Fe1–C8	2.036(7)	C11–N1–C1–C2	−146.47(0.67)
Fe1–C9	2.038(5)	O3–C13–C6–C7	175.03(0.62)
Fe1–C10	2.053(6)	C21–C20–C13–C6	−68.49(0.85)
C1–N1	1.415(8)	C21–C20–C13–O3	111.36(0.75)
N1–C11	1.423(9)		
N1–C12	1.391(8)	C1–[C1–C5]–[C6–C10]–C6	−159.8[a]
C11–O1	1.206(8)		
C12–O2	1.239(9)		
C6–C13	1.461(9)		
C13–C20	1.504(10)		
C13–O3	1.233(8)		
C21–Cl1	1.739(6)		
C25–Cl2	1.748(8)		
C1–C2	1.439(11)		
C2–C3	1.426(9)		
C3–C4	1.400(10)		
C4–C5	1.414(10)		
C5–C1	1.413(9)		
C6–C7	1.438(9)		
C7–C8	1.416(10)		
C8–C9	1.419(12)		
C9–C10	1.413(9)		
C10–C6	1.443(10)		

[a] [C1–C5] is defined as the centroid of the Cp ring C1–C5; [C6–C10] is defined as the centroid of the Cp ring C6–C10.

Å; C^9–C^{10} 1.413(9) Å; C^8–C^9 1.419(12) Å] fits to the DFT calculated data.

Having explored the structural, dynamic, optical and electrochemical properties of **2** and **3** a thermally induced melt-polycondensation [29] of **3** to a polyimine was attempted. **3** was investigated with differential scanning calorimetry in the temperature range 50–600 °C (Fig. 8). Melting of compound **3** occurs at 133 °C with $\Delta H_m = 30.7\ kJ\ mol^{-1}$. Two exothermal processes are observed peaking at 247 °C and 293 °C followed by weak endotherms at 374 °C and 479 °C. The first exotherm is associated with a mass loss of $\Delta m/m = -5.3\%$ (at 270 °C) as observed in the thermogravimetric analysis (Fig. 8) and during the second exotherm a weight loss of $\Delta m/m = -10.5\%$ is observed. Up to 460 °C a plateau is reached in the TG with a mass loss of $\Delta m/m = -20.9\%$ and at 700 °C a red material ($\Delta m/m = 20.2\%$) remains [presumably a mixture of FeO and Fe_2O_3 (calc. for FeO: $\Delta m/m = 19.2\%$); calc. for Fe_2O_3: $\Delta m/m = 21.3\%$; formed by trace oxygen present].

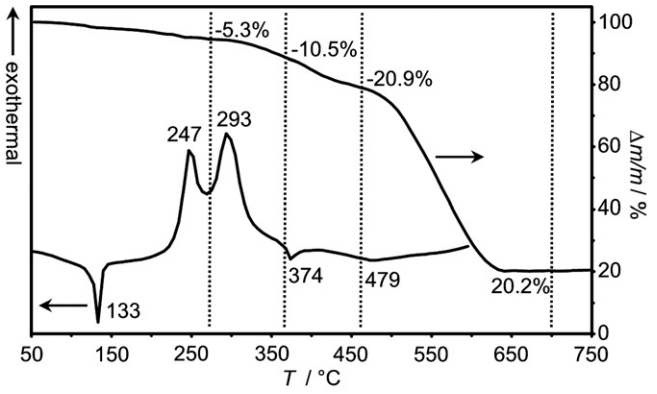

Fig. 8. DSC and TG of **3**.

The 5.3% weight loss observed at 270 °C roughly fits to the loss of one water molecule (calc. 4.8%) as would be expected for a condensation reaction. However, the analytical data recorded for the insoluble red-brown material isolated at 270 °C are inconsistent with a polyimine structure. The IR spectrum still displays a band for the C=O stretching vibration (1656 cm^{-1}), broad bands assignable to OH/NH vibrations (3140–3600 cm^{-1}), a band corresponding to aliphatic CH vibrations (2964 cm^{-1}), a band characteristic for a C–O vibration (1263 cm^{-1}) and slightly shifted signals for the C–Cl vibrations (1098, 1027 cm^{-1}; cf. **3**: 1099, 1037 cm^{-1}). A CP MAS ^{13}C NMR spectrum only reveals uncharacteristic, broad and paramagnetically shifted signals, while an EPR spectrum shows a broad signal at $g = 2.035$ ($\Delta H = 600$ G). Elemental analysis of the material indicates reduction of C, H and N content (found C 53.56, H 3.50, N 2.95%). Thus, instead of a simple condensation a more complicated mechanism is operative during the thermal decomposition of **3**. A mechanism consistent with the experimental data is proposed in Scheme 2.

In the melt the intermolecular hydrogen bonds of **3** are disrupted and intramolecular hydrogen bonds can form (**A**). In **A** the amine substituted cyclopentadienyl ring is prepared to form cyclopenta-2,4-dienylideneamine (formally by a proton/two electron transfer to the ArC(O)–CpFe fragment). The cyclopenta-2,4-dienylideneamine dissociates, rearranges to pyridine which evaporates (exothermal process, peak at 247 °C). This interpretation is also supported by the EI mass spectrum of **3** which shows a

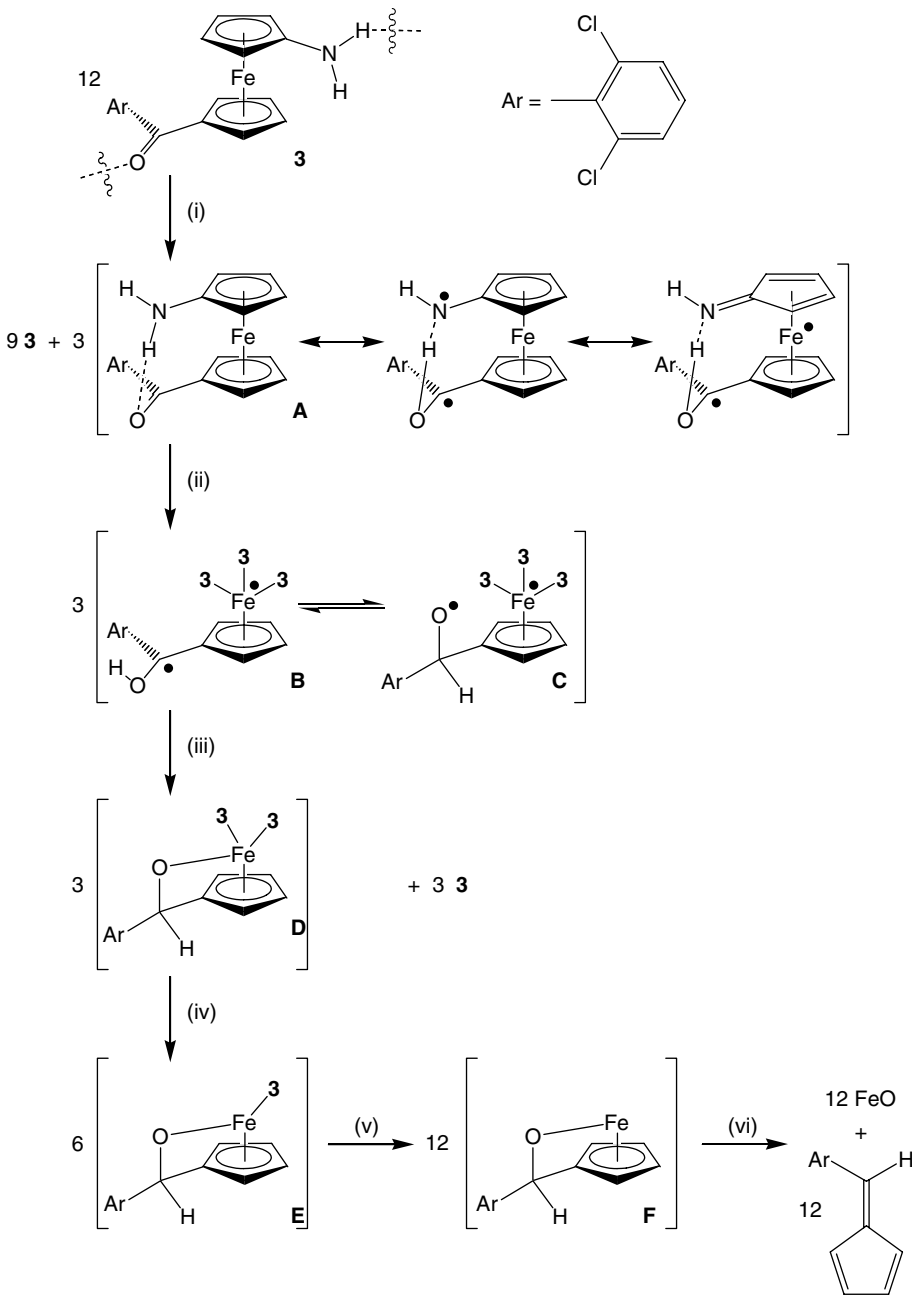

Scheme 2. Proposed thermal decomposition pathway of **3**: (i) melting at 133 °C; (ii) $-3C_5H_5N$ up to 270 °C; (iii) ligand dissociation; (iv) $-3C_5H_5N$ up to 374 °C; (v) $-6C_5H_5N$ up to 460 °C; (vi) elimination of 1,3-dichloro-2-cyclopenta-2,4-dienylidenemethyl-benzene and formation of FeO.

prominent peak at $m/z = 80.0$ for the pyridinium cation $C_5H_6N^+$. The free coordination sites at the iron centre might be occupied by remaining **3** (possibly via the C=O groups) giving the (formally) Fe^I radical species **B** (and/or its tautomer **C**) [30–33]. The elemental analysis of the isolated material **B/C** (calc. C 53.40, H 3.34, N 2.97%) fits well to the observed values (C 53.56, H 3.50, N 2.95%) as does the measured weight loss at 270 °C (obs. 5.3%; calc. for 1/4 C_5H_5N 5.3%). In addition the proposed structure accounts for the radical character (Fe^I and/or organic radical [34–37]) and the observed vibrational data (aliphatic C–H, C=O and C–O groups). During the second exotherm (peak at 293 °C) coordinated **3** dissociates from **B/C** giving **D** and another 1/4 of pyridine is liberated giving **E**. The mass loss at 360 °C (obs. 10.5%) fits to the loss of 1/2 pyridine (calc. 10.6%). After the endothermal process at 374 °C (dissociation of **3**) the remaining amine substituted cyclopentadienyl ligands are liberated as pyridine up to the plateau at 460 °C giving species **F** (observed weight loss 20.9% at 460 °C; calc. weight loss 21.1%). Finally the aryl substituted fulvene is liberated leaving iron(II)oxide.

Although not amenable to polycondensation in the melt **3** might be a useful precursor for other 1,*n*′-disubstituted ferrocene derivatives, especially for the use in catalysis and redox-active materials. Work into this direction is currently in progress.

3. Experimental

3.1. General

Unless noted otherwise, all manipulations were carried out under argon or dinitrogen by means of standard Schlenk techniques. All solvents were dried by standard methods and distilled prior to use. 2-Ferrocenylisoindole-1,3-dione (**1**) was prepared by a literature method [16]. All other reagents were used as received from commercial sources.

NMR: Varian Unity Plus 400 at 399.89 MHz (^{1}H) and 100.543 MHz (^{13}C); chemical shifts (δ) in ppm with respect to residual solvent peaks as internal standards: CD_2Cl_2 (^{1}H: $\delta = 5.32$; ^{13}C: $\delta = 53.5$). IR spectra were recorded on a BioRad Excalibur FTS 3000 spectrometer using CaF_2 cells or CsI disks. UV/Vis/NIR spectra were recorded on a Perkin Elmer Lambda 19, 0.2 cm cells (Hellma, suprasil). Cyclic voltammetry was performed using a glassy carbon electrode, a platinum electrode and a SCE electrode, 10^{-3} M in 0.1 M nBu$_4$NPF$_6$/CH_3CN, potentials are given relative to that of SCE. Mass spectra were recorded on a Finnigan MAT 8400 spectrometer. Elemental analyses were performed by the microanalytical laboratory of the Organic Chemistry Department, University of Heidelberg. Melting points were determined with a Gallenkamp capillary melting point apparatus MFB 595 010 and are uncorrected. Differential scanning calorimetry measurements were carried out on a Mettler DSC 30, heating rate 10 K min^{-1}, under argon from 30 to 600 °C. Thermogravimetric measurements were carried out on a Mettler TC 15, heating rate 10 K min^{-1} under argon from 30 to 800 °C.

3.2. Computational method

Density functional calculations were carried out with the Gaussian03/DFT [38] series of programs. The B3LYP formulation of density functional theory was used employing the LanL2DZ basis set [38]. All points were characterised as minima ($N_{imag} = 0$) or first-order saddle points ($N_{imag} = 1$) by frequency analysis.

3.3. Crystallographic structure determination

The measurements were carried out on an Enraf-Nonius Kappa CCD diffractometer using graphite monochromated Mo-Kα radiation. The data were processed using the standard Nonius software [39]. All calculations were performed using the SHELXT PLUS software package. The structure was solved using direct methods with the SHELXS-97 program and refined with the SHELXL-97 program [40]. Graphical handling of the structural data during refinement was performed using XMPA [41] and WinRay [42]. Atomic coordinates and anisotropic thermal parameters of the non-hydrogen atoms were refined by full-matrix least-squares calculations.

Crystal data for **2**: $C_{25}H_{15}Cl_2FeNO_3$, $M = 504.13$, orthorhombic space group $Pna2_1$, $a = 15.341(3)$ Å, $b = 17.090(3)$ Å, $c = 7.864(2)$ Å; $V = 2061.8(7)$ Å^3, $Z = 4$, $T = 200$ K, $\mu(MoK_\alpha) = 1.02$ mm^{-1}, 4723 reflections measured, 4542 unique, 293 parameters, $R_1(I > 2\sigma(I)) = 0.0688$ and $wR_2(F^2) = 0.1692$, Flack parameter 0.36(4), residual electron density +0.44 and −0.73 e Å^{-3}. CCDC-616594 contains the supplementary crystallographic data for this paper. These data can be obtained free of charge at www.ccdc.cam.ac.uk/conts/retrieving.html [or from the Cambridge Crystallographic Data Centre, 12 Union Road, Cambridge CB2 1EZ, UK; fax: (internat.) +44 1223/336 033; email: deposit@ccdc.cam.ac.uk].

3.4. Synthesis of 1-phthalimido-n′-(2,6-dichlorobenzoyl)-ferrocene (2)

A solution of 2-ferrocenylisoindole-1,3-dione **1** (1.6 g, 4.9 mmol) in dichloromethane (15 ml) was treated with 2,6-dichlorobenzoyl chloride (1.0 g, 4.9 mmol) and $AlCl_3$ (1.0 g, 8 mmol) at 0 °C. The resulting blue solution was stirred at 0 °C for 30 min and for additional 14 h at room temperature. The mixture was cooled to 0 °C and ice-water (30 ml) was added cautiously. The solution turned red immediately. The aqueous solution was extracted with dichloromethane (3 × 100 ml) and the combined organic phases were washed with water and 10% $NaOH_{(aq)}$. After drying over $MgSO_4$, filtration, and evaporation to dryness the crude product was obtained as a red powder. Recrystallisation from diethyl ether yielded the product as red crystals. Yield 1.74 g, 3.47 mmol (71%).

$C_{25}H_{15}Cl_2FeNO_3$ (504.15): calc. C 59.56, H 3.00, N 2.78%; found C 59.51, H 3.30, N 2.85%. IR (CsI): $\nu = 1780$ (w, CO_{sym}), 1721 (vs. CO_{asym}), 1663 (s, CO_{ketone}), 1488 (s, CN), 1095, 1036 (m, CCl) cm^{-1}. IR (CH_2Cl_2): $\nu = 1783$ (w, CO_{sym}), 1722 (vs. CO_{asym}), 1658 (s, CO_{ketone}), 1485 (s, CN) cm^{-1}. MS (EI): m/z (%) = 505 (77), 503 (92) [M^+, Cl isotope distribution], 468 (2) [M^+−Cl], 432 (4) [M^+−2Cl], 266 (100) [M^+−$C_{12}H_7Cl_2O$], 252 (6) [M^{2+}]. UV (THF): λ_{max} (ε/M^{-1} cm^{-1}) = 347 (sh, 1520), 471 (650). ^{1}H NMR (CD_2Cl_2): $\delta = 4.43$ (pt, 2H, H^{3,4}, $J = 2$ Hz), 4.63 (pt, 2H, H^{8,9}, $J = 2$ Hz), 4.69 (pt, 2H, H^{7,10}, $J = 2$ Hz), 5.11 (pt, 2H, H^{2,5}, $J = 2$ Hz), 7.28 (t, 1H, H^{23}, $^3J_{HH} = 8.5$ Hz), 7.32 (d, 2H, H^{22,24}, $^3J_{HH} = 8.5$ Hz), 7.77 (dvdvd, 2H, H^{17,18}, $^3J_{HH} = 8.3$ Hz, $^3J_{HH} = 8.25$ Hz, $^4J_{HH} = 0.85$ Hz), 7.86 (dvd, 2H, H^{16,19}, $^3J_{HH} = 8.3$ Hz, $^4J_{HH} = 0.85$ Hz). ^{13}C{^{1}H} NMR (CD_2Cl_2): $\delta = 65.0$ (s, C^{2,5}), 68.7 (s, C^{3,4}), 72.0 (s, C^{7,10}), 74.9 (s, C^{8,9}), 80.8 (s, C^6), 90.7 (s, C^1), 123.7 (s, C^{16,19}), 128.9 (s, C^{22,24}), 131.0 (s, C^{23}), 132.3 (s, C^{14,15,21,25}), 138.9 (s, C^{20}), 167.2 (s, C^{11,12}), 196.9 (s, C^{13}). Mp: 159 °C.

3.5. Synthesis of 1-amino-n′-(2,6-dichlorobenzoyl)-ferrocene (3)

1-Phthalimido-1′-(2,6-dichlorobenzoyl)-ferrocene (1.0 g, 1.98 mmol) was dissolved in dry ethanol (50 ml). Hydra-

zine monohydrate (10 ml) was added and the mixture was heated under reflux for 2 h. After cooling to ambient temperature water (100 ml) was added and the mixture was extracted with diethyl ether (3×100 ml). The combined organic phases were dried over $NaSO_4$, filtered and evaporated to dryness under reduced pressure to give a red solid. Yield: 0.64 g, 1.7 mmol (86%).

$C_{17}H_{13}Cl_2FeNO$ (374.05): calc. C 54.59, H 3.50, N 3.74%; found C 54.31, H 3.99, N 3.81%. IR (CsI): $v = 3389$, 3315 (m, NH), 1642 (s, CO_{ketone}), 1504 (m, CN), 1099, 1037 (m, CCl) cm^{-1}. IR (CH_2Cl_2): $v = 3434$, 3362 (m, NH), 1651 (s, CO_{ketone}), 1503 (m, CN). MS (EI): m/z (%) = 373 (100), 375 (64) [M^+, Cl isotope distribution], 292 (6), 294 (4) [$M^+ - C_5H_7N$, Cl isotope distribution], 80.0 (58) [$C_5H_6N^+$]. UV (CH_2Cl_2): λ_{max} ($\varepsilon/M^{-1}\,cm^{-1}$) = 362 (sh, 1375), 493 (905). ^1H NMR (CD_2Cl_2): $\delta = 2.74$ (br s, 2H, NH_2), 4.00 (pt, 2H, $H^{3,4}$), 4.05 (pt, 2H, $H^{2,5}$), 4.53 (s, 4H, $H^{7,8,9,10}$), 7.30–7.40 (m, 3H, $H^{22,23,24}$). $^{13}C\{^1H\}$ NMR (CD_2Cl_2): $\delta = 59.8$ (s, $C^{2,5}$), 66.4 (s, $C^{3,4}$), 71.6 (s, $C^{7,10}$), 74.5 (s, $C^{8,9}$), 80.5 (s, C^6), 109.1 (s, C^1), 128.9 (s, $C^{22,24}$), 130.9 (s, C^{23}), 132.4 (s, $C^{21,25}$), 139.1 (s, C^{20}), 196.9 (s, C^{13}). Mp: 133 °C.

Acknowledgement

The authors thank Dr. Otto Röhm Gedächtnisstiftung, the Fonds of the Chemical Industries, the German Science Foundation for financial support and for a Heisenberg fellowship (to K.H.). The permanent, generous support from Prof. Dr. G. Huttner is gratefully acknowledged. We thank Simone Leingang for preparative assistance.

References

[1] S.I. Kirin, H.-B. Kraatz, N. Metzler-Nolte, Chem. Soc. Rev. 35 (2006) 348–354.
[2] U. Siemeling, T.-C. Auch, Chem. Soc. Rev. 34 (2005) 584–594.
[3] N.J. Long, Metallocenes: An Introduction to Sandwich Complexes, Blackwell Science, Oxford, 1998.
[4] T.J. Peckham, P. Gómez-Elipe, in: A. Togni, R.L. Haltermann (Eds.), I. Manners in Metallocenes, Wiley-VCH, Weinheim, 1998, pp. 723–771.
[5] A. Togni, T. Hayashi (Eds.), Ferrocenes: Homogeneous Catalysis Organic Synthesis Materials Science, VCH, Weinheim, Germany, 1995.
[6] P. Nguyen, P. Gómez-Elipe, I. Manners, Chem. Rev. 99 (1999) 1515–1548.
[7] V. Balzani, A. Juris, M. Venturi, S. Campagna, S. Serroni, Chem. Rev. 96 (1996) 759–833.
[8] N.J. Long, Angew. Chem. 107 (1995) 37–56;
N.J. Long, Angew. Chem., Int. Ed. Engl. 34 (1995) 21–38.
[9] M.E. Wright, E.G. Toplikar, H.S. Lackritz, J.T. Kerney, Macromolecules 27 (1994) 3016–3022.
[10] M.E. Wright, E.G. Toplikar, Macromolecules 25 (1992) 6050–6054.
[11] R.C.J. Atkinson, V.C. Gibson, N.J. Long, Chem. Soc. Rev. 33 (2004) 313–328.
[12] L.K. Li, Y.L. Song, H.W. Hou, Y.T. Fan, Y. Zhu, Eur. J. Inorg. Chem. (2005) 3238–3249.
[13] O. Lavastre, M. Even, P.H. Dixneuf, A. Pacreau, J.-P. Vairon, Organometallics 15 (1996) 1530–1531.
[14] J.B. Heilmann, M. Scheibitz, Y. Quin, A. Sundararaman, F. Jäckle, T. Kretz, M. Bolte, H.-W. Lerner, M.C. Holthausen, M. Wagner, Angew. Chem. 118 (2006) 934–939;
J.B. Heilmann, M. Scheibitz, Y. Quin, A. Sundararaman, F. Jäckle, T. Kretz, M. Bolte, H.-W. Lerner, M.C. Holthausen, M. Wagner, Angew. Chem., Int. Ed. 45 (2006) 920–925.
[15] D. Paolucci, M. Marcaccio, C. Bruno, D. Braga, M. Polito, F. Paolucci, F. Grepioni, Organometallics 24 (2005) 1198–1203.
[16] K. Heinze, M. Schlenker, Eur. J. Inorg. Chem. (2004) 2974–2988.
[17] K. Heinze, M. Schlenker, Eur. J. Inorg. Chem. (2005) 66–71.
[18] K. Heinze, M. Beckmann, Eur. J. Inorg. Chem. (2005) 3450–3457.
[19] K. Heinze, K. Hempel, M. Beckmann, Eur. J. Inorg. Chem. (2006) 2040–2050.
[20] J. Sandstrom, J. Seita, J. Organomet. Chem. 108 (1976) 371–380.
[21] L. Lin, A. Berces, H.-B. Kraatz, J. Organomet. Chem. 556 (1998) 11–20.
[22] R.D. Moulton, A.J. Bard, Organometallics 7 (1988) 351–357.
[23] E. Roman, D. Astruc, A. Darchen, J. Organomet. Chem. 219 (1981) 221–231.
[24] S.I. Goldberg, W.D. Bailey, M.L. McGregor, J. Org. Chem. 36 (1971) 761–769.
[25] M.D. Rausch, C.A. Pryde, J. Organomet. Chem. 26 (1971) 141–146.
[26] L.R. Moffett Jr., J. Org. Chem. 29 (1964) 3726–3727.
[27] N. Weliky, E.S. Gould, J. Am. Chem. Soc. 79 (1957) 2742–2746.
[28] S. Lu, V.V. Strelets, M.F. Ryan, W.J. Pietro, A.B.P. Lever, Inorg. Chem. 35 (1996) 1013–1023.
[29] G.F. D'Alelio, W.F. Strazik, D.M. Feigl, R.K. Schoenig, J. Macromol. Sci. A2 (1968) 1457–1492.
[30] D. Astruc, Chem. Rev. 88 (1988) 1189–1216.
[31] J. Ruiz, V. Guerchais, D. Astruc, J. Chem. Soc., Chem. Commun. (1989) 812–813.
[32] J. Ruiz, D. Astruc, J. Chem. Soc., Chem. Commun. (1989) 815–816.
[33] F. Ogliaro, J.-F. Halet, D. Astruc, J.-Y. Saillard, New. J. Chem. 24 (2000) 257–259.
[34] S. Rigaut, M.-H. Delville, D. Astruc, J. Am. Chem. Soc. 119 (1997) 11132–11133.
[35] V. Guerchais, D. Astruc, J. Chem. Soc., Chem. Commun. (1984) 881–882.
[36] M.V. Rajasekharan, S. Giezynski, J.H. Ammeter, N. Oswald, P. Michaud, J.-R. Hamon, D. Astruc, J. Am. Chem. Soc. 102 (1982) 2400–2407.
[37] J.-R. Hamon, D. Astruc, P. Michaud, J. Am. Chem. Soc. 103 (1981) 758–766.
[38] M.J. Frisch, G.W. Trucks, H.B. Schlegel, G.E. Scuseria, M.A. Robb, J.R. Cheeseman, J.A. Montgomery Jr., T. Vreven, K.N. Kudin, J.C. Burant, J.M. Millam, S.S. Iyengar, J. Tomasi, V. Barone, B. Mennucci, M. Cossi, G. Scalmani, N. Rega, G.A. Petersson, H. Nakatsuji, M. Hada, M. Ehara, K. Toyota, R. Fukuda, J. Hasegawa, M. Ishida, T. Nakajima, Y. Honda, O. Kitao, H. Nakai, M. Klene, X. Li, J.E. Knox, H.P. Hratchian, J.B. Cross, C. Adamo, J. Jaramillo, R. Gomperts, R.E. Stratmann, O. Yazyev, A.J. Austin, R. Cammi, C. Pomelli, J.W. Ochterski, P.Y. Ayala, K. Morokuma, G.A. Voth, P. Salvador, J.J. Dannenberg, V.G. Zakrzewski, S. Dapprich, A.D. Daniels, M.C. Strain, O. Farkas, D.K. Malick, A.D. Rabuck, K. Raghavachari, J.B. Foresman, J.V. Ortiz, Q. Cui, A.G. Baboul, S. Clifford, J. Cioslowski, B.B. Stefanov, G. Liu, A. Liashenko, P. Piskorz, I. Komaromi, R.L. Martin, D.J. Fox, T. Keith, M.A. Al-Laham, C.Y. Peng, A. Nanayakkara, M. Challacombe, P.M.W. Gill, B. Johnson, W. Chen, M.W. Wong, C. Gonzalez, J.A. Pople, Gaussian 03, Revision B.03, Gaussian, Inc., Pittsburgh PA, 2003.

[39] R. Hooft, Collect, Data Collection Software, Nonius, The Netherlands, 1998. http://www.nonius.com.

[40] G.M. Sheldrick, SHELXS-97, Program for Crystal Structure Solution, University of Göttingen, Germany, 1997. http://www.shelx.uni-ac.gwdg.de/shelx/index.html;
G.M. Sheldrick, SHELXL-97, Program for Crystal Structure Refinement, University of Göttingen, Germany, 1997. http://www.shelx.uni-ac.gwdg.de/shelx/index.html;
International Tables for X-ray Crystallography, Kynoch Press, Birmingham, UK, vol. 4, 1974.

[41] L. Zsolnai, G. Huttner, XPMA, University of Heidelberg, Germany, 1998. Available from: <http://www.rzuser.uni-heidelberg.de/~il1/laszlo/xpm.html>.

[42] R. Soltek, G. Huttner, WinRay, University of Heidelberg, Germany, 1999; http://www.uni-heidelberg.de/institute/fak12/AC/huttner/frame/frame_soft.html.